Journal of Solid State Electrochemistry
https://doi.org/10.1007/s10008-024-05813-w

ORIGINAL PAPER

Enhanced dye degradation using 2H-MoS_2 and 1T@2H-MoS_2: A comparative study

Jitendra Jadhav[1] · Yogesh Waghadkar[2] · Yogita Padwal[3] · Mohamed Hashem[4] · Hassan Fouad[5] · Shankar S. Kekade[6] · Chiaki Terashima[7] · Ratna Chauhan[3] · Shrikant Charhate[1] · Suresh W. Gosavi[7,8,9] · Dattatray J. Late[1]

Received: 17 October 2023 / Revised: 4 January 2024 / Accepted: 15 January 2024

Abstract
Removing the organic dye from polluted water is very challenging due the human health concern and ecological environments. The photocatalytic process can remove the organic dye from polluted water under the sunlight. To enhance the photocatalytic property, here we have synthesized the MoS_2 by using two different molybdenum sources via one-step hydrothermal methods characterized using XRD, FESEM, Raman, XPS and UV-Visible techniques. We investigate the potential of synthesized MoS_2 nanostructures for dye degradation applications. The results demonstrate that both 2H-MoS_2 and 1T@2H-MoS_2 exhibit remarkable photocatalytic degradation capabilities towards the model dye. However, the 1T@2H-MoS_2 hybrid structure outperforms 2H-MoS_2, exhibiting significantly enhanced photocatalytic activity and faster dye degradation kinetics. The improved performance of 1T@2H-MoS_2 can be accredited to its wide absorption in solar spectrum, effective charge separation, and increased active sites resulting from the 1T phase incorporation. The photocatalytic activity of 2H-MoS_2 shown 73% and 1T@2H-MoS_2 exhibits 98% methylene blue dye degradation in 60.0 min and5.0 min under the visible range of sunlight respectively. Overall, this study highlights the potential of 2D MoS_2 nanostructures, particularly the 1T@2H-MoS_2 hybrid, as efficient catalysts for dye degradation. The development of such materials offers promising prospects for the remediation of dye-contaminated wastewater and contributes to the advancement of sustainable environmental technologies.

Keywords 2H-MoS_2 · 1T@2H-MoS_2 · Two-dimensional (2D) · Photocatalytic activity · Dye degradation · Wastewater treatment

✉ Ratna Chauhan
ratnasingh.bhu@gmail.com

✉ Suresh W. Gosavi
swg@physics.unipune.ac.in

✉ Dattatray J. Late
datta099@gmail.com

[1] Centre for Nanoscience and Nanotechnology, Amity School of Engineering and Technology, Amity University Maharashtra, Panvel, Mumbai, Maharashtra 410206, India

[2] Department of Electronics and Instrumentation Science, Savitribai Phule Pune University, Ganeshkhind, Pune 411007, India

[3] Department of Environmental Science, Savitribai Phule Pune University, Pune 411007, India

[4] Dental Health Department, College of Applied Medical Sciences, King Saud University, Riyadh 11433, Saudi Arabia

[5] Applied Medical Science Department, Community College, King Saud University, P.O. Box 10219, Riyadh 11433, Saudi Arabia

[6] Radhabai Kale Mahila Mahavidyalaya, Ahmednagar 414001, India

[7] Photocatalysis International Research Center, Research Institute for Science & Technology, Tokyo University of Science, 2641 Yamazaki, Noda, Chiba 278-8510, Japan

[8] School of Chemistry, University of Melbourne, Parkville, VIC 3010, Australia

[9] Department of Physics, Savitribai Phule Pune University, Pune 411 007, India

Introduction

Recently, water pollution is a major problem because of its serious impact on human health as well as ecological environments. Water pollution is caused by various sectors, such as industries, paint, printing, textiles, etc. [1, 2]. As a result, there is a need to treat wastewater and remove contaminants from water. To overcome these issues, several efforts have been made, but photocatalytic activity is the most promising method to remove organic dye from water under sunlight. Removing organic dyes such as methylene blue, methylene orange, rhodamine, etc. is very challenging. Numerous efforts have been made to remove organic dye from water by using metal oxides such as WO_3, ZnO, MoO_3, NiO, TiO_2, etc. [3–7]. However, the major challenge of these metal oxides is the optical absorption of UV light due to wide band gap [8]. This wide bandgap also limits the performance of photocatalytic activity within the visible range. To tackle these issues, transition metal chalcogenides (TMD) are the most promising and most suitable candidates for photocatalytic activity in the visible range because they are narrow bandgap semiconductors [9]. amongst all TMD materials, molybdenum disulfide (MoS_2) is the most favourable material for photocatalytic activity [9]. MoS_2 has good electrical conductivity, optical and electrical properties, a narrow bandgap, and layer structure and 2D morphology, which is unusual. Molybdenum atoms are packed between pairs of sulphur atoms in a layered structure to form MoS_2 [10–14]. So, the band gap of MoS_2 can be altered by varying the layer of MoS_2, and mostly the band of monolayer MoS_2 exhibits 1.8 eV [15]. These narrow band gaps enable visible absorption, generate electron-hole pairs, and make MoS_2 a special material for organic dye degradation [16]. But the problem doesn't end here, though MoS_2 has several merits, there are a few demerits also. Mostly, in MoS_2, during the photocatalytic activity, there is quick recombination of the exciton generated by a photon, which reduces the rate of dye degradation [17–20]. Furthermore, does the 2 H phase of MoS_2 provide the tremendous electron conveyance kinetics property to enhance the conductivity of MoS_2, which is very challenging for photocatalytic activity. Tuning the optical bandgap and morphology will also enhance the photocatalytic performance under sunlight. Several efforts have been made to improve photocatalytic performance up to this point. Lie Tian et al. created 2H-MoS_2, which demonstrated a catalytic efficiency of 56.3% after 2 h of visible light irradiation [21]. S.V.P. Vattikuti et al. used wet chemical methods to prepare MoS_2 multiwall and achieved 84% dye degradation in 60 min [22, 23].

In this report, we have successfully synthesized the 2H-MoS_2 and hybrid phases of the 1T@2H-MoS_2 nanoflower by using two different molybdenum sources via a single-step hydrothermal method. Further, various characterization methods such as XRD, FESEM, FT-IR, and Raman spectroscopy have been performed to examine the characteristics of synthesized materials. For the application part, the photot-catalytic dye degradation (methylene blue) was performed under the sunlight. Both materials are highly efficient for removing dye from polluted water, but the nanostructured 1T@2H-MoS_2 shows a more outstanding photocatalytic property than the 2H-MoS_2 nanoflowers. The hybrid phases 1T@2H-MoS_2 that show 98% methylene blue dye degradation in 5 min under direct sunlight. Reportedly, this works represents the fastest methylene blue dye degradation under the sunlight by using pristine MoS_2 nanostructures.

Experimental

Materials and chemicals

Ammonium molybdate 99% AR, Sodium molybdate dihydrate 99% AR, Methylene blue (MB) and Thiourea AR are purchased from Merck, India. DI water was used for all the experiments.

Synthesis of MoS_2

The MoS_2 were synthesized by one-step facile hydrothermal methods. The 0.2 M precursor for Mo (precursor for 2H-MoS_2 and 1T@2H-MoS_2 is Sodium molybdate dihydrate and ammonium molybdate respectively) and 0.2 M thiourea were added in 70 ml of DI water and stirred for half an hour for the homogeneous solution. Then, the above-prepared solution was transferred in 100 ml of Teflon autoclave for 24 h at 180ºC followed by natural cooling till room temperature and washed with DI water and ethanol till pH neutral. Further, the product was dried in an electric oven at 80 ºC for 12 h. The obtained product was named 2H-MoS_2 and 1T@2H-MoS_2.

Photocatalytic studies

The photocatalytic performance of synthesized **MoS_2** were tested in natural sunlight. 25 mg of **2H-MoS_2 and 1T@2H-MoS_2** photocatalyst was mixed into 50 mL of Methylene Blue dye solution (10 ppm) for this experiment. The above reaction mixture of dye and catalyst were stirred in dark for 30 min to achieve the adsorption/desorption equilibrium. After stirring in dark the reaction mixture was placed in natural sunlight with constant stirring. To evaluate the % degradation, the dye solution was collected at regular interval until the solution of MB become colourless.

With the help of UV-Vis spectrophotometer the absorption intensity were measured for all the collected samples and the degradation of MB (%) was calculated using equation given below:

$$\text{Degradation}\,(\%) = \frac{c_o - c_t}{c_o} \times 100\% \quad (1)$$

Where C_o & C_t = initial and concentration after time t of MB solution after illumination.

Characterizations

The crystal structure analysis of 2H-MoS_2 and 1T@2H-MoS_2 was done by X-Ray diffraction (Bruker D2 phasor) in 2θ range between 5° to 80° in ambient conditions. The morphological investigation was performed with NOVA FESEM, NPE303. The chemical structural investigation was performed by Raman spectroscopy, Thermo Scientific spectrometer, with LASER 532 nm excitation line. Further, the functional groups were studied by FT-IR spectroscopy using Jasco FT/IR-6100 from 400 cm^{-1} to 4000 cm^{-1} and absorption spectroscopy was performed range between 200 and 800 nm by using a Jasco spectrometer (670). The XPS were performed by PHI 5000 Versaprobe-II ULVAC-PHI INC instrument with a monochromatized Mg (K-alpha: E = 1253.6 eV).

Results and discussion

FESEM

The morphological investigation was performed with FESEM as represented in Fig. 1. Figure 1 (a & b) represents the FESEM image of 2H-MoS_2, which displays the MoS_2 agglomerated nanostructures were grown homogeneously. Further, at higher magnification, the 2H-MoS_2 image at 500 nm scale reveals the MoS_2 nanosheet is agglomerated together and formed the flower like nanostructures. Figure 1 (c & d) shows the FESEM image of 1T@2H-MoS_2, which reveals that MoS_2 are formed nanoflower-like morphology and this nanoflower-like morphology is formed by agglomeration of various MoS_2 nanosheets. Figure 1 also represents the elemental analysis and EDS analysis of 2H-MoS_2 and 1T@2H-MoS_2 supports the presence of Mo and S with no impurities.

TEM

Transmission Electron Microscopy (TEM) analysis provided detailed insights into the structural features of both 2H-MoS_2 and 1T@2H-MoS_2 materials, corroborating the FESEM observations in Fig. 1. The TEM images of 2H-MoS_2 exhibited agglomerated nanostructures, consistent with the FESEM findings, revealing MoS_2 nanosheets arranged in a flower-like morphology at a higher magnification of 200 nm (Fig. 2). In contrast, TEM imaging of 1T@2H-MoS_2 showcased distinctive nanoflower-like morphologies formed through the agglomeration of multiple MoS_2 nanosheets, validating the FESEM observations. Additionally, the Selected Area Electron Diffraction (SAED) patterns for both materials revealed crystalline structures characterized by diffraction spots indicative of the hexagonal lattice structures of 2H-MoS_2 and the coexistence of 1T and 2 H phases in 1T@2H-$_{MoS2}$, further supporting the phase purity and crystalline nature of the synthesized materials.

UV-Visible spectroscopy

The optical property of synthesized MoS_2 were studied by UV-Visible spectroscopy range between 200 and 800 nm as represented in Fig. 3 (a, b).

The optical direct band of 1T@2H-MoS_2 and 2H-MoS_2 was investigated by the Tauc's plot as represented in equation (a). Figure 3 (a) shows the Tauc's plot of 1T@2H-MoS_2 and Fig. 3 (b) shows the Tauc's plot of 2H-MoS_2 and the inset represents the absorbance (%) vs. wavelength of 2H-MoS_2. Whereas and the inset id absorbance (%) vs. wavelength.

$$\alpha h\nu = B(h\nu - E_g)^n \quad (2)$$

Where, α is coefficient of absorption, E_g is band gap energy, n = ½, ¼ or 2 is coefficient, B is constant of proportionality and h is Planck's constant. The optical direct band of 2H-MoS_2 and 1T@2H-MoS_2 are 2.21 eV and 1.99 eV respectively.

Structural investigations and XRD

Figure 4 illustrating the schematic representation for the MoS_2. 1T@2H-MoS_2 represents a mixed crystal structure, where the 1T phase is merged into the 2 H phase. The 1T phase is typically incorporated into the 2 H structure by introducing defects or applying strain to the crystal lattice. The resulting 1T@2H-MoS_2 structure combines the properties of both the 1T and 2 H phases, offering unique properties and enhanced functionalities. The crystal structure-property of 2H-MoS_2 and 1T@2H-MoS_2 were studied by XRD as shown in Fig. 5 (a, d).

The XRD analysis confirms a precise match between the spectra of 2H-MoS_2 and JCPDS file no. 73-1508, aligning peaks at 2θ values of 12.2°, 32.6°, 35.3°, and 57° with the

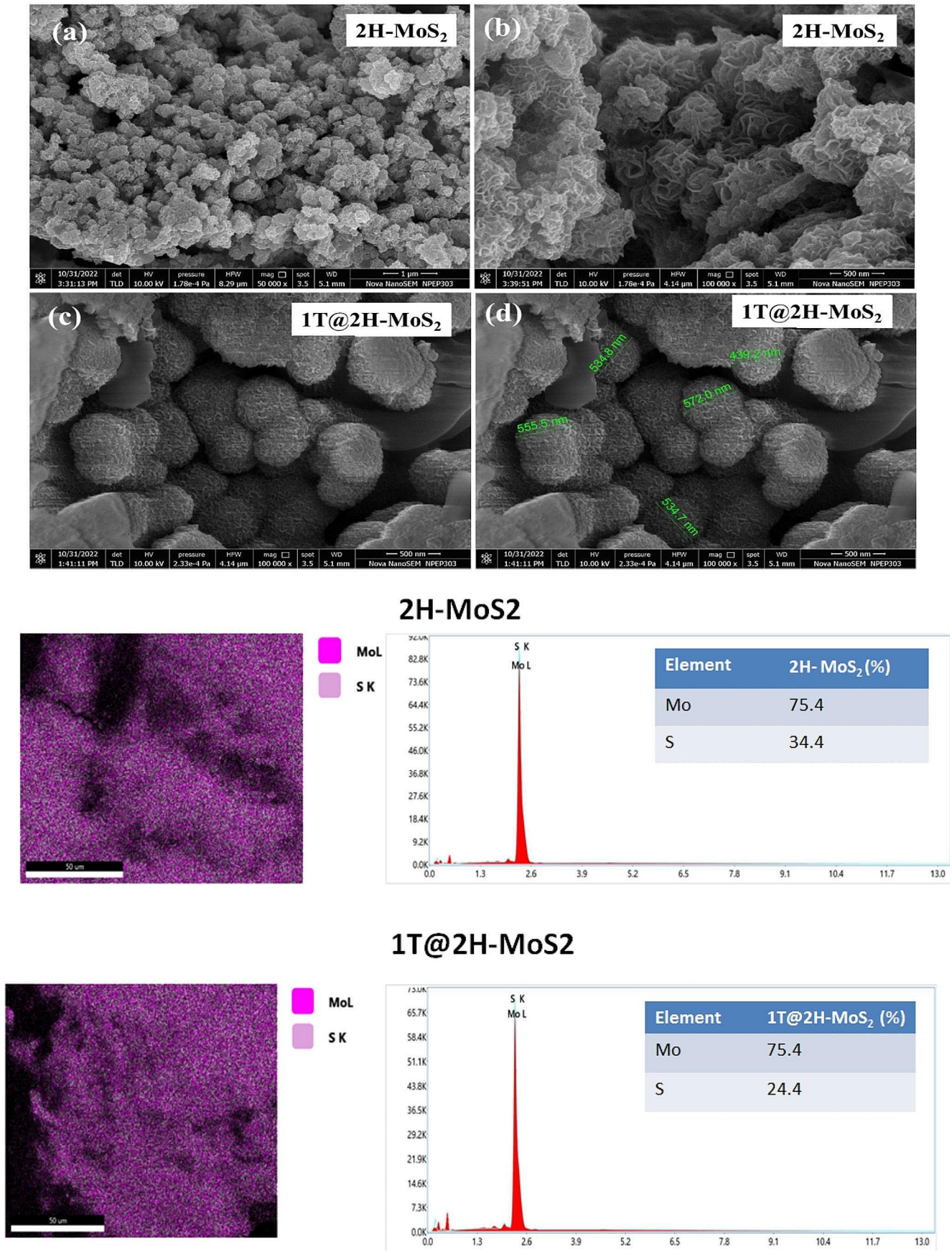

Fig. 1 FESEM images of 2H-MoS_2 (**a**, **b**) and 1T@2H-MoS_2 (**c**, **d**); Elemental mapping and EDS analysis of 2H-MoS_2 and 1T@2H-MoS_2

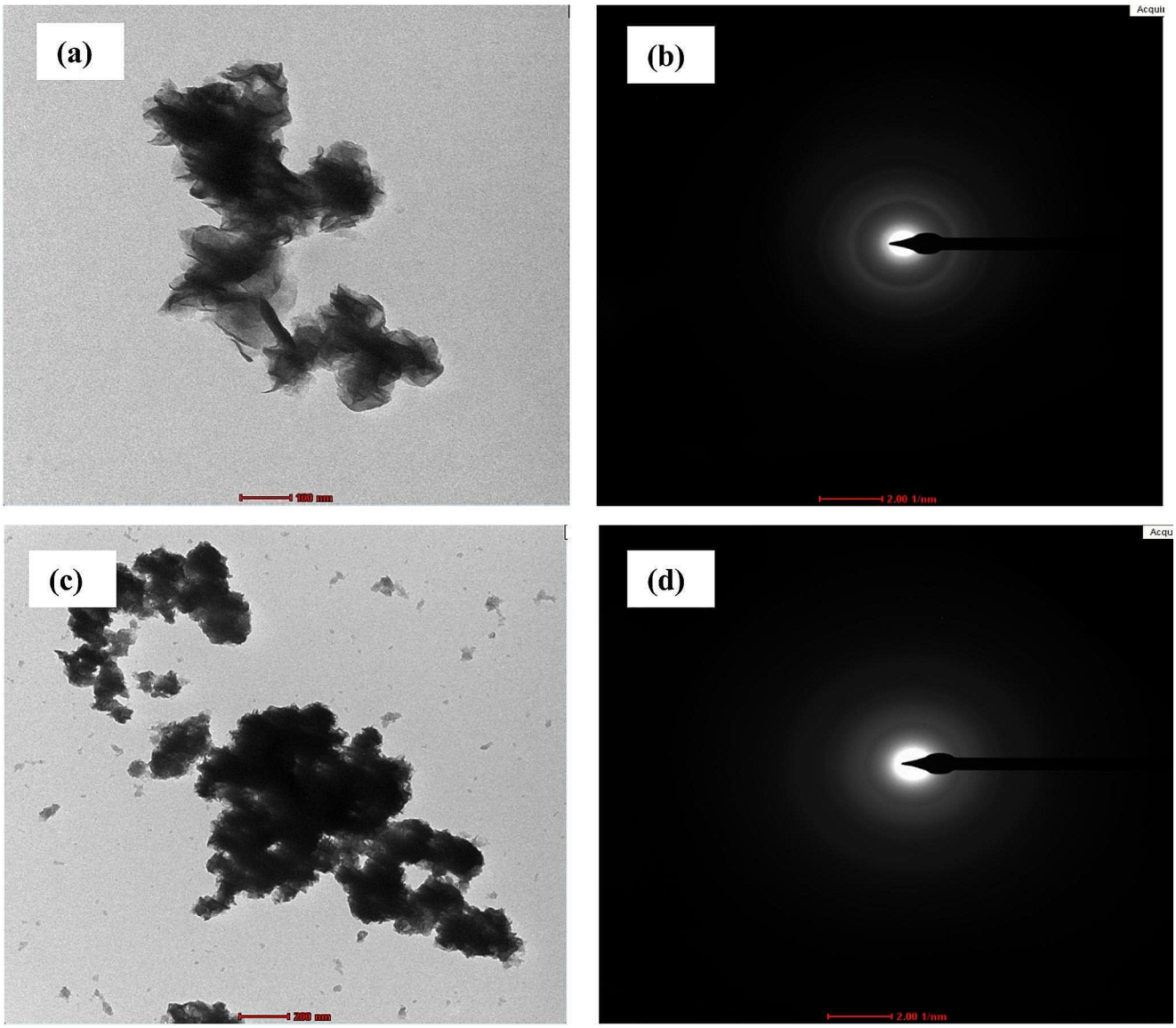

Fig. 2 TEM images and SEAD pattern of 2H-MoS_2 (**a**, **b**) and 1T@2H-MoS_2 (**c**, **d**)

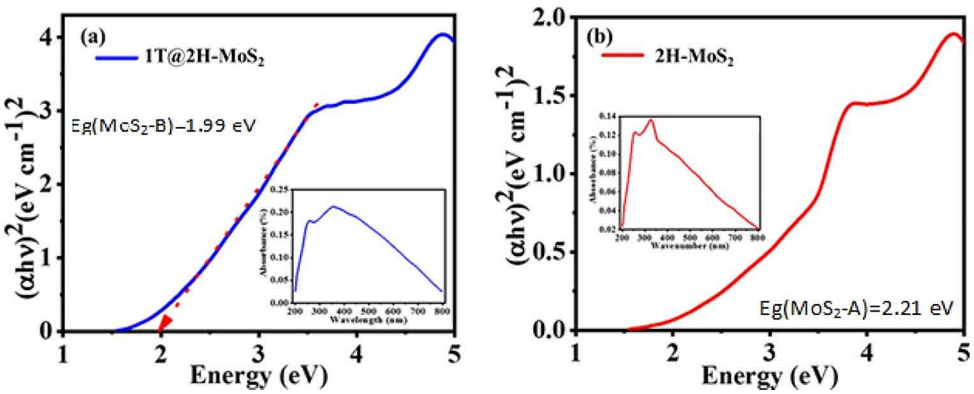

Fig. 3 (**a**) Tauc's plot of 1T@2H-MoS_2 and inset is absorbance wavelength of 1T@2H-MoS_2 and (**b**) Tauc's plot of 2H-MoS_2 and inset is absorbance vs. wavelength of 2H-MoS_2

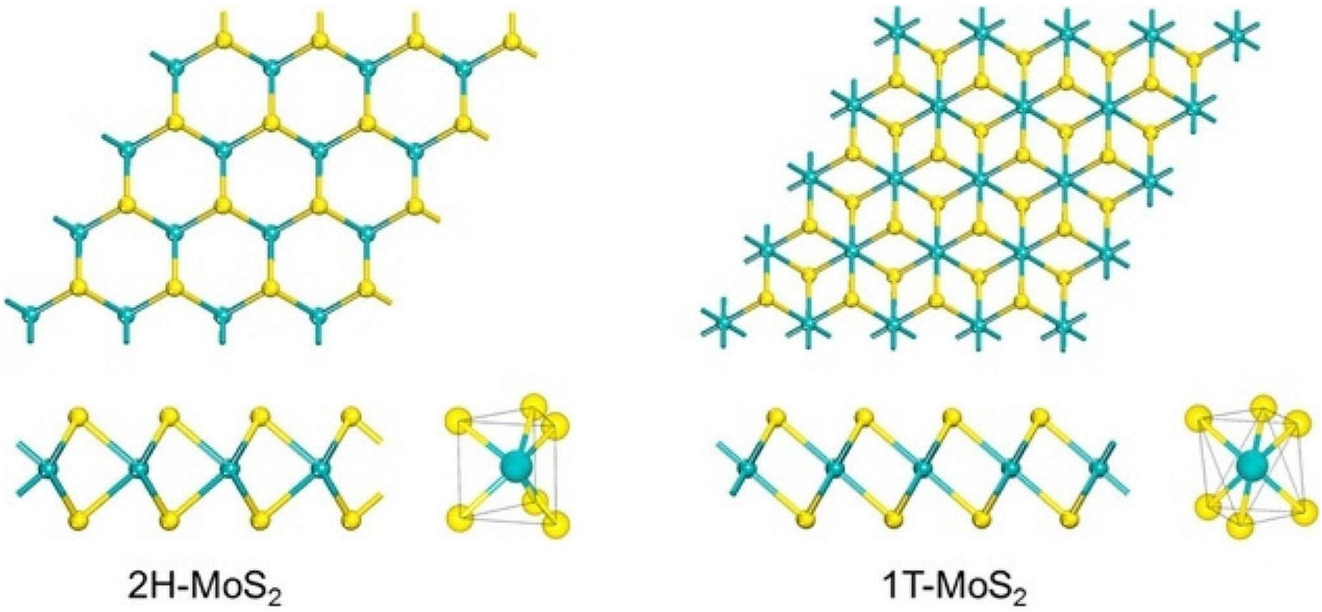

Fig. 4 Top and side views of the 2 H (left) and 1T (right) structures for the MoS_2 monolayer. The trigonal prism coordination for the Mo atom in 2H-MoS_2 and the octahedral coordination for the Mo atom in 1T-MoS_2 are also shown. Mo, cyan; S, yellow

(002), (100), (101), and (110) planes of the 2 H@MoS2 nanostructure (Fig. 5a). Correspondingly, the XRD patterns of 1T@2H-MoS_2 align with JCPDS file numbers 37-1492, showcasing distinctive peaks at 2θ values of 9.10°, 31.05°, 43.2°, and 58.15°, attributed to the (002), (100), (006), and (110) planes (Fig. 5d). These findings affirm the crystalline nature of MoS2 with a hexagonal crystal structure, devoid of any obvious impurity peaks.

Raman Study

The chemical structural property of 2H-MoS_2 and 1T@2H-MoS_2 were studied by Raman spectroscopy as represented in Fig. 5b. The Fig. 5 (b) shows the Raman spectra of 2H-MoS_2, Peaks at 221.45 cm^{-1}, 374.25 cm^{-1}, and 402.7 cm^{-1} attributed to E1g, E2g, and A1g respectively due to the 2 H phase of MoS_2 [24]. Especially, E1g is due to the acoustic longitudinal phonon modes and E2g and A1g are due to the Raman active in-plane and out-plane of the 2 H phase respectively [25–27]. The existence of additional peaks at 195 cm^{-1} (J1), 219 cm^{-1} (J2), and 335 cm^{-1} (J3) in the Raman spectra of 1T@2H-MoS_2 indicates distinct phonon modes characteristic of 1T-MoS_2. This observation strongly suggests the coexistence of a noteworthy proportion of the 1T phase alongside the prevalent 2H-MoS_2 phase within the sample.

FTIR Study

The functional group and vibration mode of prepared materials were studied by FT-IR spectroscopy as shown in Fig. 5 (c, f). The FT-IR spectra for the 2H-MoS_2 at 589.12 cm^{-1} reveals the stretching vibration of Mo-S. The peak between 732.2 cm^{-1} to 1372.12 cm^{-1} is attributed to C-S and C = S (Fig. 5c). Whereas, a higher wavenumber peak at 1664.23 cm^{-1} is due to the stretching mode of O-H for hydroxyl group chemisorb water molecules [26–28]. Figure 5 (f) shows the FT-IR spectra of 1T@2H-MoS_2 and spectra at 455.91 cm^{-1}, 1435.85 cm^{-1}, 1680.43 cm^{-1}, and 3553.19 cm^{-1} are attributed to the bending vibration of Mo-S, stretching vibration of C-O, at high wavenumber due to the symmetrical stretching vibration for hydroxyl group respectively [29, 30].

XPS Study

To know the chemical components and oxidation states of 1T@2H MoS_2 and 2H-MoS_2, X-ray photoelectron spectroscopy measurement was carried out. Figure 6 (a) shows the XPS survey scan of 2H-MoS_2, confirm the existence of Mo and S. Figure 6 (b and c) shows the deconvoluted XPS spectra of Mo 3d and S 2p, which validate the presence of Mo and S in 2H-MoS_2. In the case of 2 H –MoS_2 sample, the Mo 3d spectrum shows the two peaks observed at 228 eV and 232 eV. Both peak deconvoluted into 4 peaks denoted by A, B, C and D at observed at 228.6 eV, 229.6 eV, 231.7 eV and 232.7 eV respectively. Peak A and C assign to 1T MoS_2

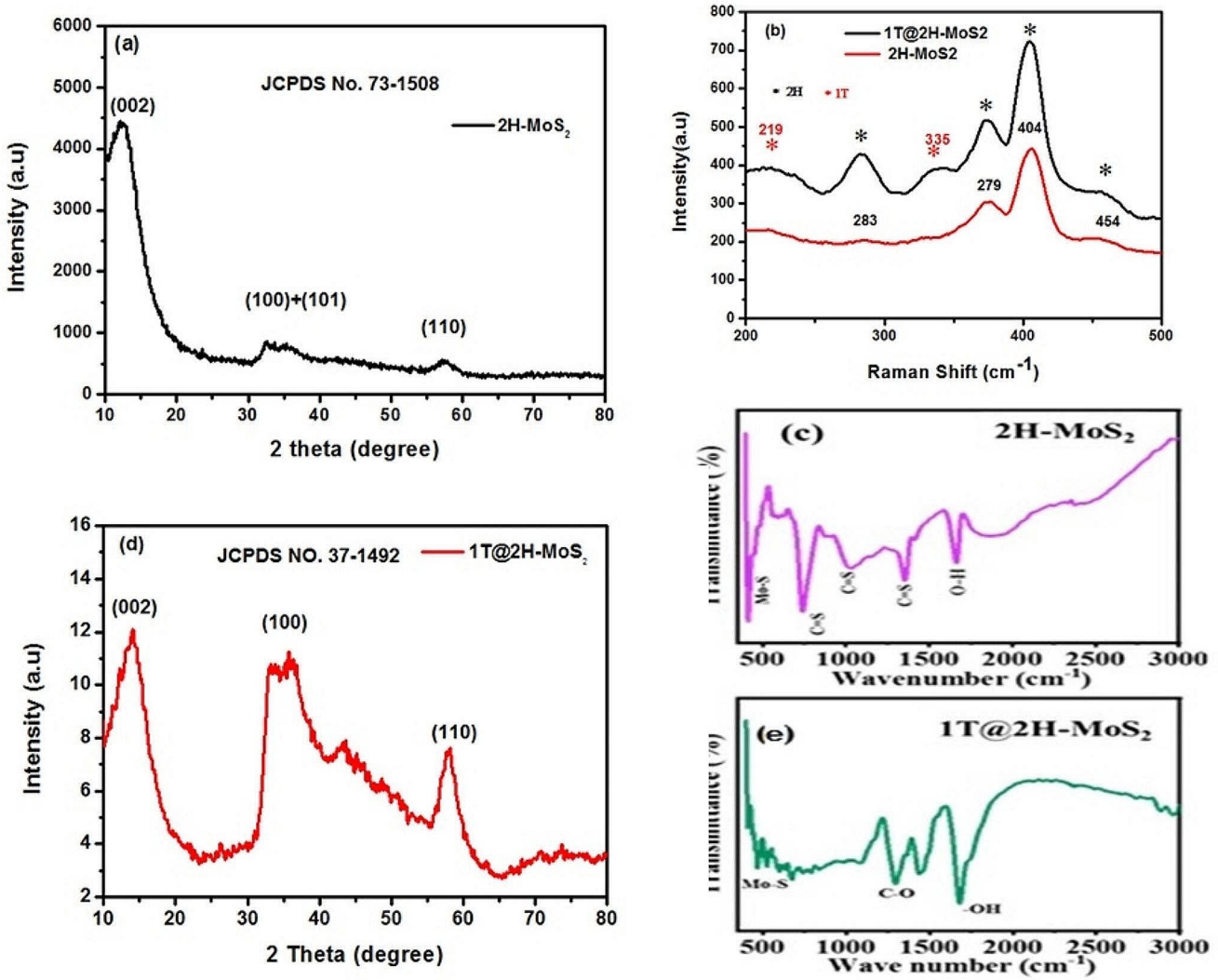

Fig. 5 (**a**, **d**) XRD spectra of 2H-MoS_2 and 1T@2H-MoS_2, (**b**) Raman spectra of 2H-MoS_2 and 1T@2H-MoS_2, and (**c**, **e**) FT-IR spectra of 2H-MoS_2 and 1T@2H-MoS_2

whereas the peak B and D assign to 2H-MoS_2 compound. The high-resolution S 2p spectrum shows two peaks at 161.5 and 162.7 eV respectively which corresponds to S $2p_{3/2}$ and S $2p_{1/2}$. Here both Mo 3d and S 2p peak reveals to 2 H phase of MoS_2 [31, 32].

Figure 6 (d) exhibiting scan of 1T@2H-MoS_2 and reveals the presence of Mo and S in the sample, while, Fig. 6 (e and f) illustrating the deconvoluted XPS of Mo 3d and S 2p for the 1T@2H-MoS_2. In 1T-2 H MoS_2 sample, the XPS spectra doublet of Mo 3d deconvoluted into 4 peaks A, B, C and D at 228.7, 229.6, 231.9 and 232.7 eV. The Peak A and C reveals the 1T-MoS_2 phase whereas the peak B and D reveals the 2H-MoS_2 phase. In both the samples of Mo at the low binding energy, the Mo shows the 4 + oxidation state of Mo (Peak A and C) and the higher binding energy peaks (B and D) shows the Mo^{6+} state. The spin orbit splitting energy for both Mo^{4+} and Mo^{6+} is 3.2 eV and 3.1 eV which is well matches with standard data. The S2p spectra for 1T@2H-MoS_2 deconvoluted into three peaks A, B, C at 161.5, 162.9 and 163.7 eV. The peak A and B assigned to S $2p_{3/2}$ and S $2p_{1/2}$ resp. The peak C observed at higher binding energy corresponds to S-O bonding in the sample. It is observed that the binding energy of 1T-MoS_2 phases is 0.9 eV lower than the 2 H MoS_2 phase.

In Fig. 6 (g), the XPS scan of 1T@2H-MoS_2 post-use as a catalyst indicates the presence of Mo (Molybdenum) and S (Sulfur) elements within the sample. Subsequently, Fig. 6 (h) and 6 (i) depict the deconvolution of the Mo 3d and S 2p XPS spectra, respectively, for the 1T@2H-MoS_2 material. The comparison between pre- and post-use XPS spectra showed consistent peaks and binding energies, suggesting that the material retained its chemical integrity after interacting with pollutants. This observation indicates that there were no significant alterations in the electronic structure or

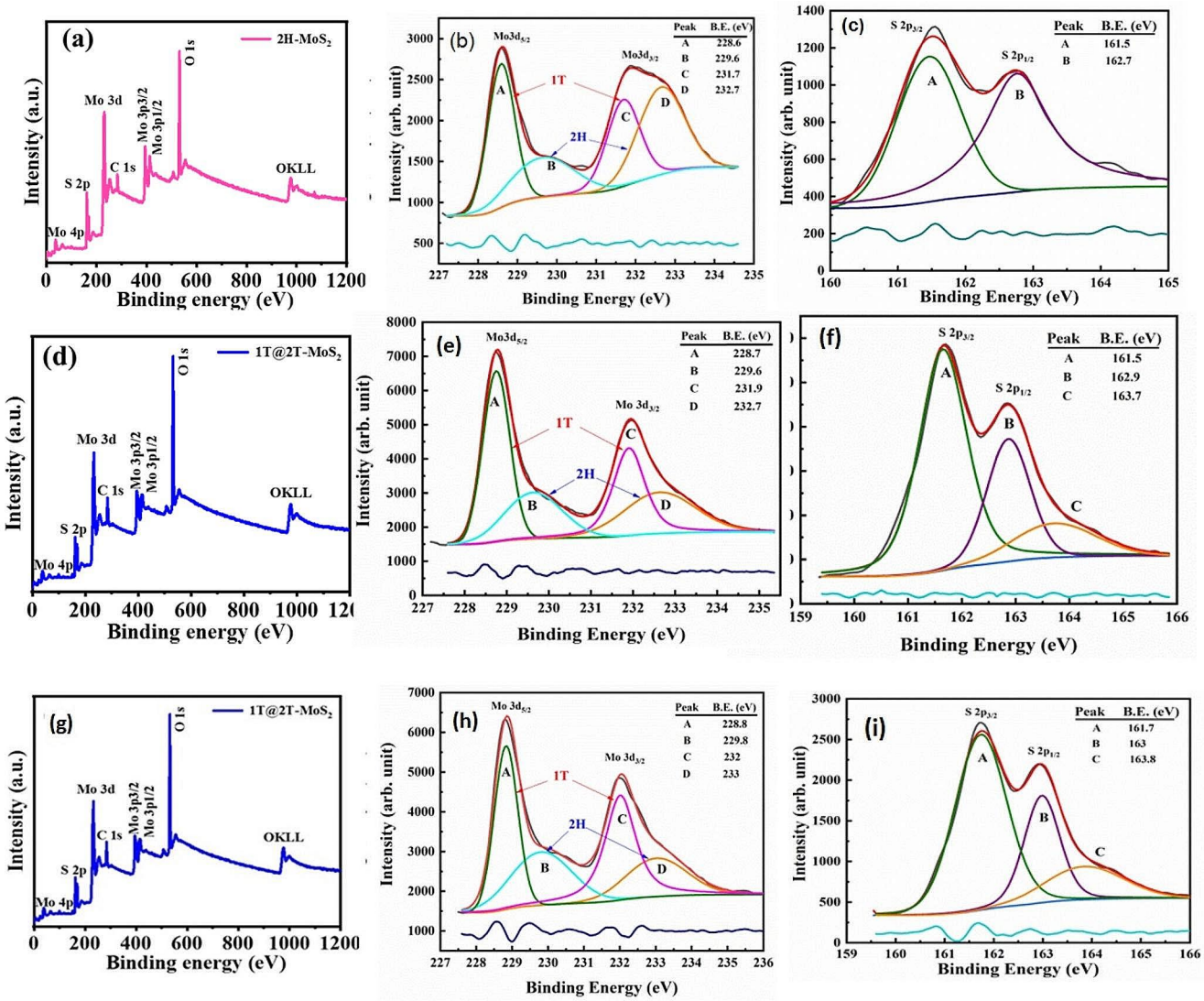

Fig. 6 (**a**) XPS spectra of survey scan of 2H-MoS_2, (**b**, and **c**) Deconvoluted XPS spectra of Mo 3d and S 2p, (d) XPS spectra survey scan of 1T@2H-MoS_2 (**e**, and **f**) Deconvoluted XPS spectra of 1T@2H-MoS_2 Mo 3d and S 2p (**Before use as catalyst; d, e, f**), (**g**) XPS spectra survey scan of 1T@2H-MoS_2 (**h**, and **i**) Deconvoluted XPS spectra of 1T@2H-MoS_2 Mo 3d and S 2p (**After use as catalyst; g, h, i**)

surface composition of 1T@2H-MoS_2 due to the pollutant interaction.

Photocatalytic property

The synthesized MoS_2 were examined for the photocatalytic activity in the MB dye degradation under the sunlight. In photocatalytic activity, the interface between adsorbate and adsorbent is a very crucial factor to limit or tune the efficiency and selectivity of adsorbent components. To full fill, these requirements nano-structured MoS_2 are the most promising materials for the high adsorption capacity material, especially MoS_2 nano-sheets. The methylene blue dye in aqueous solution degradation was carried out under the sunlight using 2H-MoS_2 and 1T@2H-MoS_2 as catalyst as represented in Fig. 7 (a & b).

Figure 7 (a) shows the methylene blue degradation in an aqueous solution at various time intervals under the sunlight. The 2H-MoS_2 shows the 100% absorbance spectra during the 0 min time interval and after 60 min exposure of sunlight it shows 73% degradation in 60 min. Figure 7 (b) shows the MB degradation with 1T@2H-MoS_2 as photocatalyst. In the presence of 1T@2H-MoS_2 the MB was completely degraded with 5 min. Figure 7 (c and d) shows the methylene blue degradation kinetics at various time intervals (graph of ln (C_t/C_o) vs. Time (min) of 2H-MoS_2 and 1T@2H-MoS_2.

The kinetic parameters of photo-catalytic MB dye degradation using 2H-MoS_2 and 1T@2H-MoS_2 catalyst can

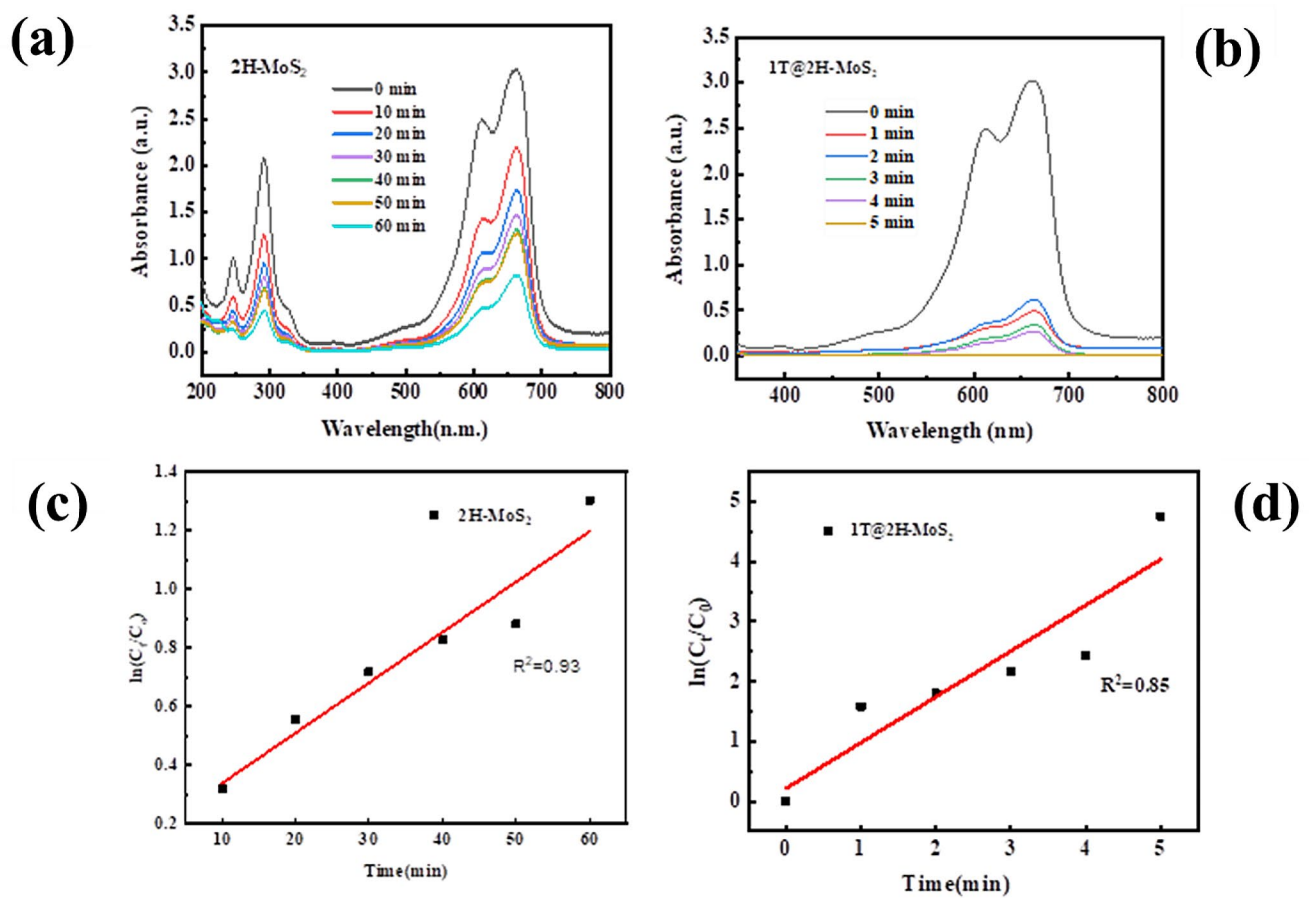

Fig. 7 UV absorption spectra of Methylene Blue after photocatalytic degradation using (**a**) 2H-MoS_2 (**b**) 1T@2H-MoS_2: ln (Ct/Co) Vs. time plot of MB for (**c**) 2H-MoS_2 (**d**) 1T@2H-MoS_2

be calculated using Langmuir– Hinshelwood equation of kinetic model [22, 23] as follows:

$$\ln(\frac{C_t}{C_o}) = -kt + B$$

Where B, k and t represent the constant, rate constant of degradation (min^{-1}) of dye, and reaction time respectively. The k (rate constant) is assessed from the slope of the plot. The graph exhibits a linear relationship, which can be fitted to a suitable kinetic model, first-order model or the Langmuir-Hinshelwood model for kinetic parameters calculations.

The corresponding regression coefficient (R^2) for the experiment is also calculated. The R^2 values for the experiments are found to be 0.93 and 0.85 for 2H-MoS_2 and 1T@2H-MoS_2 respectively, representing that the dye degradation satisfy the first order kinetics.

The crystal structure of 2H-MoS_2 and the incorporation of the 1T phase in 1T@2H-MoS_2 play a substantial role in defining their properties. These structures influence the bandgap, electrical conductivity, optical properties, and catalytic behaviour of the materials. The higher degradation efficiency of 1T@2H-MoS_2 can be attributed to several factors. Firstly, the incorporation of the 1T phase in 1T@2H-MoS_2 introduces distortions in the crystal structure, leading to an increased number of active sites and enhanced catalytic properties. The distorted octahedral coordination of molybdenum in the 1T phase facilitates the adsorption and activation of the MB dye molecules, promoting their degradation. Secondly, the 1T@2H-MoS_2 structure may provide improved charge transfer and separation characteristics compared to 2H-MoS_2. The presence of the 1T phase can enhance the conductivity of the material and facilitate efficient charge carrier mobility, reducing the recombination of photoinduced electron-hole pairs. This enhanced charge transfer capability contributes to the accelerated degradation of the MB dye. Additionally, the unique branched and petal-like structure of the nanoflowers formed by 1T@2H-MoS_2 offers a larger surface area and increased exposure of active sites, promoting the adsorption and degradation of MB molecules. The performance of 1T@2H-MoS_2 is better than the individual moiety [33]. The intricate morphology of the nanoflowers provides additional pathways for efficient mass transfer and diffusion of reactants, further enhancing

the photocatalytic performance. The incorporation of the 1T phase, along with the unique nanoflower morphology, significantly accelerates the degradation process, making 1T@2H-MoS_2 a promising candidate for advanced photocatalytic applications requiring rapid and efficient dye degradation. By understanding and manipulating the crystal structures, researchers can tailor the properties of 2H-MoS_2 and 1T@2H-MoS_2 for various applications, such as electronics, optoelectronics, catalysis, and energy storage.

Mechanism of dye degradation and reusability studies for 1T@2H-MoS_2

The high photocatalytic efficiency observed in 1T/2H-MoS_2 nanostructures is likely attributable to a specific mechanism outlined in Fig. 8. This proposed mechanism posits that 2H-MoS_2 functions as an efficient photosensitizer while the metallic 1T-MoS_2 phase acts as a co-catalyst, enhancing electron transfer processes. Upon illumination, electron-hole pairs generated within 2H-MoS_2, exploiting its narrow bandgap. Electrons (e_{CB}^-) are stimulated from the valence band (VB) to the conduction band (CB) of 2H-MoS_2, thereby generating holes (h_{VB}^+) in the VB (Eq. 3). Subsequently, photogenerated electrons become entrapped by 1T-MoS_2, noticeably restricting their recombination rate and prolonging the duration of the redox reaction. This phenomenon facilitates the conversion of O_2 molecules into O_2^{*-} (Eq. 4). As adsorbed O_2 engages in multi-electron and proton redox reactions (Eqs. 5 and 6), it culminates in the formation of OH* molecules, favourably promoting the photocatalytic degradation of MB (Eq. 7).

$$1T@2HMoS_2 + hv \rightarrow h_{VB^+} + e_{CB^-} \quad (3)$$

$$e^- + O_2 \rightarrow O_2^{*-} \quad (4)$$

$$O_2 + 2e^- + 2H^+ \rightarrow H_2O_2 \quad (5)$$

$$H_2O_2 + e^- + H^+ + hv \rightarrow OH^* + H_2O \quad (6)$$

$$O_2^{*-}, OH^*h^+ + MBdye \rightarrow CO_2 + H_2O + inorganicmolecule \quad (7)$$

The reusability of the photocatalyst was evaluated through four repeated cycles. Catalyst (1T@2H-MoS_2) was extracted after use, then washed twice and dried. The dried powder was again utilized to degrade the methylene blue dye. In this set of experiments, ratio of catalyst and dye were maintained same in all cycles. It was observed that the degradation of MB was decreased from 100%, 98%, 84% and 44% at the end of every cycle (Fig. 9).

Conclusions

The work reported the successful synthesis of MoS_2 by one-step hydrothermal methods and evaluated its performance as photocatalyst. Further, the morphological investigation was performed by FESEM imaging and crystal structural investigation was performed by the XRD spectra, reveals 2H-MoS_2 nanostructured and 1T@2H-MoS_2 nanoflower-like morphology along with hexagonal crystal structure. Additionally, the optical direct bandgap of 2H-MoS_2 and 1T@2H-MoS_2 is 2.21 eV and 1.99 eV was calculated by the

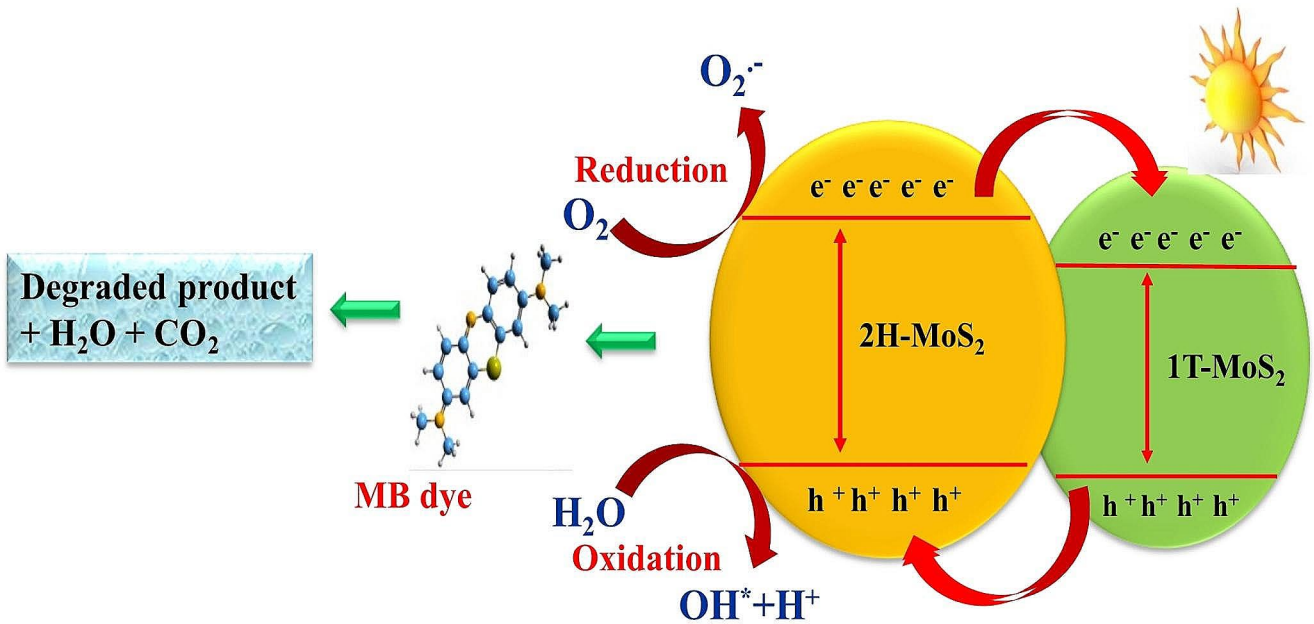

Fig. 8 Mechanism of methylene blue dye degradation by 1T@2H-MoS_2

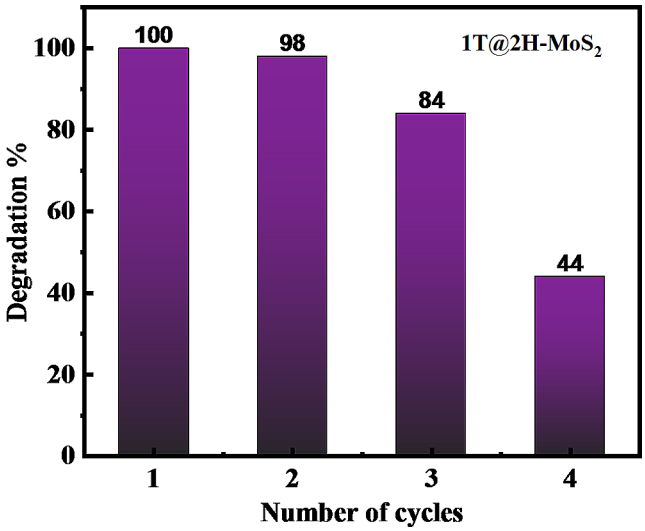

Fig. 9 Photocatalysis reusability performance of 1T@2H-MoS_2

Tauc's plot. The photocatalytic adsorption and degradation using 1T@2H-MoS_2 were ~98% in 5.0 min and 2H-MoS_2 nanoflower exhibits 73% methylene blue dye degradation in 60 min under the sunlight. The crystal structure of 2H-MoS_2 and the incorporation of the 1T phase in 1T@2H-MoS_2 have been found to significantly influence the properties of the nanoflowers. The unique crystal structures, such as the hexagonal lattice arrangement in 2H-MoS_2 and the distorted octahedral coordination in the 1T phase, contribute to the distinctive physical, chemical, and electronic properties exhibited by these nanoflowers.

Acknowledgements Authors would like to acknowledge the Savitribai Phule Pune University, BARC, and National centre for Nanoscience's and Nanotechnology, University of Mumbai for the central characterization facility.

Author contributions Mr. Jitendra Jadhav: Experimental investigation including synthesis of materials, photocatalytic activity. Ms. Yogita Padwal: photocatalytic activity. Data curation, Writing - original draft. Dr. Yogesh Waghadkar: Formal analysis. Prof. Mohamed Hashem: Formal analysis, Interpretation of measurements. Prof. Hassan Fouad: Formal analysis, Interpretation of measurements. Dr. Shankar S. Kekade: Formal analysis, Interpretation of measurements. Prof. Chiaki Terashima: Formal analysis, Interpretation of measurements. Dr. Ratna Chauhan: Formal analysis, Interpretation of measurements. Prof. Shrikant Charhate: Formal analysis, Interpretation of measurements. Prof. Suresh W. Gosavi: Conceptualization, Investigation, Formal analysis, Supervision. Dr. Dattatray J. Late: Conceptualization, Investigation, Formal analysis, Supervision.

Funding The author would like to extend their sincere appreciation for funding this research to Researchers supporting project number (RSP2024R117), King Saud University, Riyadh, Saudi Arabia.

Data availability The data will be available from the authors with reasonable request.

Declarations

Conflict of interest There is no conflict of interest.

References

1. Raman CD, Kanmani S (2016) Textile dye degradation using nano zero valent iron: a review. J Environ Manage 177:341–355
2. Ao K, Li D, Yao Y et al (2018) Fe-doped Co9S8 nanosheets on carbon fiber cloth as pH-universal freestanding electrocatalysts for efficient hydrogen evolution. Electrochim Acta 264:157–165
3. Gupta SP, Nishad H, Magdum V, Walke PS (2020) High-performance supercapacitor electrode and photocatalytic dye degradation of mixed-phase WO3 nanoplates. Mater Lett 281
4. Shen W, Li Z, Wang H et al (2008) Photocatalytic degradation for methylene blue using zinc oxide prepared by codeposition and sol-gel methods. J Hazard Mater 152:172–175
5. Etman AS, Abdelhamid HN, Yuan Y et al (2018) Facile Water-based strategy for synthesizing MoO3-x nanosheets: efficient visible light photocatalysts for Dye Degradation. ACS Omega 3:2201–2209
6. Sabouri Z, Akbari A, Hosseini HA, Darroudi M (2018) Facile green synthesis of NiO nanoparticles and investigation of dye degradation and cytotoxicity effects. J Mol Struct 1173:931–936
7. Keerthana SP, Yuvakkumar R, Ravi G et al (2022) Investigation of optimum mn dopant level on TiO2 for dye degradation. Chemosphere 306:135574
8. Balasubramaniam B, Singh N, Kar P et al (2019) Engineering of transition metal dichalcogenide-based 2D nanomaterials through doping for environmental applications. Mol Syst Des Eng 4:804–827
9. Zhang R, Wan W, Li D et al (2017) Three-dimensional MoS2/reduced graphene oxide aerogel as a macroscopic visible-light photocatalyst. Cuihua Xuebao/Chinese Journal of Catalysis 38:313–320
10. Yuan Y, Shen P, Li Q et al (2017) Excellent photocatalytic performance of few-layer MoS2/graphene hybrids. J Alloys Compd 700:12–17
11. Jaleel RM, Pinheiro UC JR D, et al (2022) Architecture of visible-light induced Z-scheme MoS2/g-C3N4/ZnO ternary photocatalysts for malachite green dye degradation. Environ Res 214:113742
12. Wang C, Zhan Y, Wang Z (2018) TiO2, MoS2, and TiO2/MoS2 heterostructures for Use in Organic dyes Degradation. ChemistrySelect 3:1713–1718
13. Yuan Y, Guo R, tang, Hong L, fei et al (2021) Recent advances and perspectives of MoS2-based materials for photocatalytic dyes degradation: a review. Colloids Surf a 611:125836
14. Panchal D, Sharma A, Pal S (2023) Engineered MoS2 nanostructures for improved photocatalytic applications in water treatment. Mater Today Sustain 21
15. Tian L, Wu R, Liu HY (2019) Synthesis of Au-nanoparticle-loaded 1T@2H-MoS 2 nanosheets with high photocatalytic performance. J Mater Sci 54:9656–9665
16. Vattikuti SVP, Byon C (2016) Bi2S3 nanorods embedded with MoS2 nanosheets composite for photodegradation of phenol red under visible light irradiation. Superlattices Microstruct 100:514–525
17. Liang J, Wang C, Zhao P et al (2018) Interface Engineering of anchored ultrathin TiO2/MoS2 heterolayers for highly-efficient Electrochemical Hydrogen production. ACS Appl Mater Interfaces 10:6084–6089. https://doi.org/10.1021/acsami.7b19009

18. Ma L, Hu Y, Zhu G et al (2016) In situ thermal synthesis of inlaid ultrathin MoS2/Graphene Nanosheets as Electrocatalysts for the hydrogen evolution reaction. Chem Mater 28:5733–5742. https://doi.org/10.1021/acs.chemmater.6b01980
19. Liang J, Li J, Zhu H et al (2016) One-step fabrication of large-area ultrathin MoS2 nanofilms with high catalytic activity for photovoltaic devices. Nanoscale 8:16017–16025. https://doi.org/10.1039/C6NR03635J
20. Naik SS, Lee SJ, Theerthagiri J et al (2021) Rapid and highly selective electrochemical sensor based on ZnS/Au-decorated f-multi-walled carbon nanotube nanocomposites produced via pulsed laser technique for detection of toxic nitro compounds. J Hazard Mater 418:126269. https://doi.org/10.1016/j.jhazmat.2021.126269
21. Theerthagiri J, Lee SJ, Karuppasamy K et al (2021) Application of advanced materials in sonophotocatalytic processes for the remediation of environmental pollutants. J Hazard Mater 412:125245. https://doi.org/10.1016/j.jhazmat.2021.125245
22. Theerthagiri J, Park J, Das HT et al (2022) Electrocatalytic conversion of nitrate waste into ammonia: a review. Environ Chem Lett 20:2929–2949. https://doi.org/10.1007/s10311-022-01469-y
23. Yu Y, Min A, Jung HJ et al (2021) Method development and mechanistic study on direct pulsed laser irradiation process for highly effective dechlorination of persistent organic pollutants. Environ Pollut 291:118158. https://doi.org/10.1016/j.envpol.2021.118158
24. Yao Y, Ao K, Lv P, Wei Q (2019) MoS2 coexisting in 1T and 2H phases synthesized by common hydrothermal method for hydrogen evolution reaction. Nanomaterials 9:1–12
25. Vishnoi P, Sampath A, Waghmare UV, Rao CNR (2017) Covalent functionalization of nanosheets of MoS2and MoSe2by substituted benzenes and other Organic molecules. Chem---Eur J 23:886–895
26. Naresh Kumar T, Chandrasekaran N, Lakshminarasimha Phani K (2015) Structural and electronic modification of MoS2 nanosheets using S-doped carbon for efficient electrocatalysis of the hydrogen evolution reaction. Chem Commun 51:5052–5055
27. Abareshi A, Bafkari R, Houshiar M, Dinarvand R (2021) Molybdenum disulfide/carbon nanocomposite with enhanced photothermal effect for doxorubicin delivery. Eur Phys J Plus 136:1–16
28. Feng X, Tang Q, Zhou J et al (2013) Novel mixed-solvothermal synthesis of MoS2 nanosheets with controllable morphologies. Cryst Res Technol 48:363–368
29. Dos Santos ML, Lima RC, Riccardi CS et al (2008) Preparation and characterization of ceria nanospheres by microwave-hydrothermal method. Mater Lett 62:4509–4511
30. Graham GW, Weber WH, Peters CR, Usmen R (1991) Empirical method for determining CeO2-particle size in catalysts by raman spectroscopy. J Catal 130:310–313
31. Liang J, Zhu G, Wang C et al (2017) MoS2-Based all-purpose Fibrous Electrode and Self-Powering Energy Fiber for Efficient Energy Harvesting and storage. Adv Energy Mater 7:1601208. https://doi.org/10.1002/aenm.201601208
32. Chi J-Q, Chai Y-M, Shang X et al (2018) Heterointerface engineering of trilayer-shelled ultrathin MoS2/MoP/N-doped carbon hollow nanobubbles for efficient hydrogen evolution. J Mater Chem A 6:24783–24792. https://doi.org/10.1039/C8TA08753A
33. Chen M, Sun T, Zhao W, Yang X et al (2021) In situ growth of metallic 1T-MoS_2 on TiO_2 nanotubes with Improved Photocatalytic performance. ACS Omega 19:12787. https://doi.org/10.1021/acsomega.1c01068